Direct observation of tiers in the energy landscape of a chromoprotein: A single-molecule study

Clemens Hofmann*, Thijs J. Aartsma†, Hartmut Michel‡, and Jürgen Köhler*§

*Experimental Physics IV and Bayreuther Institut für Makromolekülforschung, University of Bayreuth, 95440 Bayreuth, Germany; †Department of Biophysics, Huygens Laboratory, Leiden University, P.O. Box 9504, 2300 RA, Leiden, The Netherlands; and ‡Department of Molecular Membrane Biology, Max Planck Institute of Biophysics, Marie-Curie Strasse 15, 60439 Frankfurt am Main, Germany

Edited by Peter G. Wolynes, University of California at San Diego, La Jolla, CA, and approved October 22, 2003 (received for review June 24, 2003)

Single-molecule spectroscopic techniques were applied to individual pigments embedded in a chromoprotein. A sensitive tool to monitor structural fluctuations of the protein backbone in the local environment of the chromophore is provided by recording the changes of the spectral positions of the pigment absorptions as a function of time. The data provide information about the organization of the energy landscape of the protein in tiers that can be characterized by an average barrier height. Additionally, a correlation between the average barrier height within a distinct tier and the time scale of the structural fluctuations is observed.

Proteins are supramolecular machines that perform a tremendous variety of tasks in living organisms, such as the transport of electrons and small molecules, catalysis of biochemical reactions, or storage of energy to fuel metabolic processes. Despite the multitude of functions associated with proteins, they all consist of a linear chain of covalently linked amino acids. The high specificity of a particular protein results from its complex three-dimensional structure. The primary polypeptide sequence folds into secondary structural elements, such as α-helices and β-sheets, and the secondary structures are folded into a compact three-dimensional tertiary arrangement that determines the biological role and the status of activity of the protein. Proteins are remarkably robust despite the fact that their structure is stabilized only by relatively weak peptide–peptide and protein–solvent interactions, such as hydrogen bonds and hydrophobic interactions. The connection among protein folding, protein structure, and protein function is one of the greatest challenges of current research. A major question that arises is: how does a protein fold within a reasonable time into its biologically active form?

Even for a small protein consisting of $\approx$100 amino acids, the number of possible conformations is $\approx 10^{100}$. Because of the weak interactions that stabilize the protein and the many degrees of freedom of such a large molecule, the lowest energy state is not unique, and description in terms of a rugged energy landscape is appropriate. The term "energy landscape" refers to the potential energy hypersurface of $\approx$ 3,000 dimensions, resulting from the coordinates of the atoms of the protein. It features a large number of minima, maxima, and saddle points, and each minimum in this landscape represents a different conformational substate (CS) that corresponds to a different arrangement of the atoms. However, the number of possible conformations of a protein is so large that folding into the native state within a reasonable time by a process of statistical trial and error is impossible (Levinthal's paradox). The contemporary picture is that protein folding occurs by a progressive stabilization of intermediates that retains partially "correct" folding units guided by interactions that stabilize subdomains and domains of the final folded state.

To describe protein dynamics and function, a model has been put forward that proposes that the energy landscape is arranged in hierarchical tiers. On each level of the hierarchy, the CSs are characterized by the average energy barriers between them, which decrease with the descending hierarchy (1–3). A consequence implied by this idea is that structural fluctuations of a protein become organized hierarchically and that biological processes are described in terms of characteristic temperature-dependent rate distributions associated with different tiers. Supporting evidence for this concept has been obtained from experimental work on heme proteins (1, 4–9) and the photosynthetic reaction center (10). The structural heterogeneity and dynamics in hemeproteins were investigated by studying the reaction dynamics of ligand rebinding to myoglobin after flash photolysis, following the pioneering work by Frauenfelder and coworkers (11). In the case of photosynthetic reaction centers, the effect of structural adaptation on charge recombination was investigated. In both cases, energy tiers could be identified in the interplay between protein dynamics and structural function.

Because conformational fluctuations of the protein are equivalent to the rearrangements of its atoms, chromophores embedded in the protein experience those changes as fluctuations in the local interactions that are strongly distance-dependent. As a consequence, the pigments react to conformational changes of the protein with changes of their electronic energies, making them suited to monitor the dynamics of a protein with optical spectroscopy. Valuable information about the dynamics of proteins and the related time scales has been obtained by persistent spectral hole-burning spectroscopy (7, 12–14).

Here, we report the observation of CSs in single-molecule experiments on light-harvesting complex 2 (LH2) complexes from *Rhodospirillum molischianum*. The salient feature of this technique is that it allows us to elucidate information that is commonly washed out by ensemble averaging in bulk measurements, by allowing direct observation of the dynamics of molecular processes without the need for synchronization of events.

Briefly, LH2 is a pigment–protein complex that serves as a peripheral light-harvesting antenna in bacterial photosynthesis (15–17). It comprises 808 amino acids, has a molecular mass of 100 kDa, and is 9 nm in diameter and 5 nm in height. The structure of this complex has been obtained by x-ray crystallography with atomic resolution (18) and is displayed in Fig. 1*A Upper*. It features a highly symmetric assembly that comprises 24 bacteriochlorophyll (BChl) *a* molecules arranged in two concentric rings (Fig. 1*A Lower*). One ring consists of a group of eight well separated BChl *a* molecules (B800), which absorb light at $\approx$800 nm (12,500 cm^{-1}). The other ring consists of 16 closely interacting BChl *a* molecules (B850), which absorb light at $\approx$850 nm (11,765 cm^{-1}). Fig. 1*B* displays several fluorescence-excitation spectra of LH2 from *Rs. molischianum* that were recorded at 1.4 K. The top traces in Fig. 1*B* show the comparison between an ensemble spectrum (red) and the sum of 24 spectra recorded from individual complexes (black). The lower three

This paper was submitted directly (Track II) to the PNAS office.

Abbreviations: BChl, bacteriochlorophyll; CS, conformational substate; LH2, light-harvesting complex 2; *Rs. molischianum*, *Rhodospirillum molischianum*.

§To whom correspondence should be addressed. E-mail: juergen.koehler@uni-bayreuth.de.

www.pnas.org/cgi/doi/10.1073/pnas.2533896100

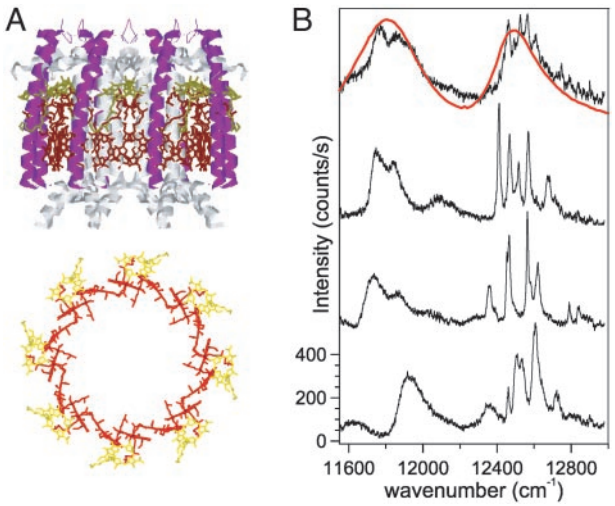

Fig. 1. Single-molecule fluorescence-excitation spectroscopy. (*A*) X-ray structure of the peripheral LH2 complex from *R. molischianum* as determined by Koepke *et al*. (18) (*Upper*) and top view of the arrangement of the BChl *a* molecules in the pigment protein complex (*Lower*). The protein backbone has been omitted for clarity. The B800 (yellow) and B850 (red) chromophores are shown. (*B*) Fluorescence-excitation spectra of LH2 complexes from *Rs. molischianum*. The top traces show the comparison between a room temperature ensemble absorption spectrum (red) and the sum of 24 fluorescence-excitation spectra recorded from individual complexes (black). The lower three traces display spectra from individual LH2 complexes. Each spectrum has been averaged over all possible excitation polarizations. The vertical scale is valid for the lowest trace; all other traces were offset for clarity. All spectra were recorded at 1.4 K with an excitation intensity of 10 W/cm^2.

traces display spectra from individual LH2 complexes. Spectroscopy of individual LH2 complexes reveals a striking difference between the two absorption bands. The B850 band is dominated by a few broad absorptions that reflect the exciton character of the involved electronic excitations, whereas the B800 band consists of several narrow lines that vary from complex to complex with respect to both the number of lines and their spectral positions. These absorptions correspond to excitations that are mainly localized on individual BChl *a* molecules (19–23).

In this article, we focus on the spectroscopy of the B800 chromophores as local probes, which can be used to monitor changes in the local protein environment. Such changes can be induced by optical excitation of the chromophore and subsequent decay of the excited state. Because of the low fluorescence quantum yield of LH2 of ≈10% (24), a large fraction of the average absorbed energy is dissipated by radiationless decay, resulting in the excitation of nuclear motions of the protein matrix. On relaxation back to thermal equilibrium, there is a finite probability that the system ends up in a different CS, which is reflected by a change in transition energy of the chromophore. The photon energy that is dissipated in this way, ≈1.5 eV (1 eV = 1.602×10^{-19} J) in the case of the B800 chromophores, exceeds by far the thermal energy kT, where k is Boltzmann's constant and T is the thermodynamic temperature of 1.4 K at which the measurements are performed. Therefore, the space of the CSs that is probed by the induced structural fluctuations is not restricted to the part of the energy landscape that is accessible under thermal equilibrium. In contrast to the examples of hemeproteins and photosynthetic reaction centers mentioned above, which involve a perturbation of the system far from equilibrium, our approach entails a momentary excitation of nuclear motion and a subsequent relaxation back to thermal equilibrium.

Experimental Methods

LH2 complexes of *Rs. molischianum* were prepared as described (25). To study individual complexes, thin polymer films were prepared by adding 1.8% (wt/wt) poly(vinyl alcohol) (M_r = 125,000 g/mol) to a solution of 5×10^{-11} M LH2 in buffer (20 mM Tris/0.1% lauryl dimethylamine-*N*-oxide, pH 8). A drop (10 μl) of this solution was spin-coated on a lithium fluoride substrate (15 s at 500 rpm, followed by 60 s at 2,000 rpm), producing high-quality films with a thickness of <1 μm. The samples were mounted immediately in a liquid-helium bath cryostat and cooled to 1.4 K.

To perform fluorescence-excitation spectroscopy, the samples were excited by a continuous-wave tunable titanium-sapphire laser through a home-built microscope. To obtain a well defined variation of the wavelength of the laser, the intracavity birefringent filter has been rotated with a motorized micrometer. For calibration purposes, a wave meter (ExFo Burleigh, Victor, NY) has been used, and we verified the accuracy and reproducibility of 1 cm^{-1} for the laser frequency. A fluorescence-excitation spectrum of an individual LH2 complex was obtained in two steps. First, a wide-field image was taken of the sample by excitation at 800 nm and fluorescence detection at 880 nm with a charge-coupled device camera (512 SB, Roper Scientific, Trenton, NJ). From this image, a spatially well isolated complex was selected. Next a fluorescence-excitation spectrum of this complex was obtained by switching to the confocal mode of the microscope and scanning the excitation wavelength while detecting fluorescence at 880 nm with a single-photon-counting avalanche photodiode (SPCM-AQR-16, Perkin–Elmer). The detection bandwidth was 20 nm. The spectra were obtained by repetitive scanning of the whole spectral range at a high rate and by storing the different traces separately. With an acquisition time of 10 ms per data point, this method yields a nominal resolution of 0.5 cm^{-1}, ensuring that the spectral resolution is determined by the bandwidth of the laser (1 cm^{-1}).

Experimental Results

High-resolution optical spectra of the B800 chromophores were obtained by recording fluorescence-excitation spectra of the B800 band from individual LH2 complexes in rapid succession. An example is shown in Fig. 2*A* in a two-dimensional representation, in which the horizontal axis corresponds to photon energy, the vertical axis corresponds to time, and the grayscale corresponds to the absorption intensity. The spectrum that results when the whole sequence is averaged is displayed in Fig. 2*B*. The sequential data acquisition scheme enables us to follow the intensities of the individual spectral features as a function of time. Interestingly, we found strong intensity fluctuations of the individual B800 absorptions. As an example, we refer to the two absorptions at 12,921 cm^{-1} and 12,642 cm^{-1} (Fig. 2*A*, a and a′, respectively). The time dependence of their emission intensity is shown in more detail in Fig. 2*C*. For both resonances, the signal exhibits abrupt changes from up to 6,000 cps to the background level. From visual inspection, it seems that the traces are anticorrelated. Indeed, this conjecture is supported by the auto- and cross-correlations of the two trajectories (Fig. 2*D*). Both autocorrelations drop within the temporal resolution of this experiment to an average value of 0, a sign that the observed intensity fluctuations are uncorrelated on this time scale. In contrast, the cross-correlation shows a clear dip around $t = 0$, which shows unambiguously that the two absorption lines, separated by 278 cm^{-1}, are closely associated. Similar changes in transition energy by several hundred wave numbers have been observed also for the pair of absorptions (Fig. 2*A*, b and b′), and details are given in Table 1 for three pairs of absorptions from another LH2 complex. Those spectral changes occur at a rate of

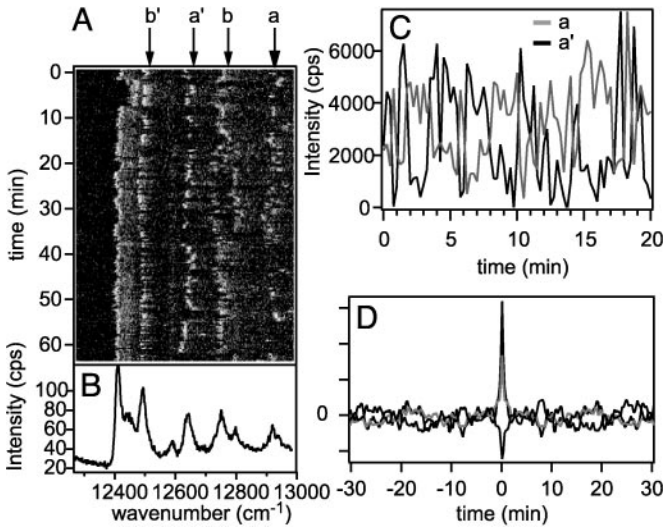

Fig. 2. Large spectral changes of the B800 absorptions. (*A*) Time sequence of 256 consecutively recorded fluorescence-excitation spectra stacked on top of each other. The fluorescence intensity is indicated by the grayscale. (*B*) Average of the stack of spectra shown in *A*. (*C*) Intensity of the fluorescence as a function of time for the spectral features (a and a′), as displayed in *A*. (*D*) Autocorrelation (upper solid gray and black lines for a and a′, respectively) and cross-correlation (lower solid black line) of the absorptions a and a′.

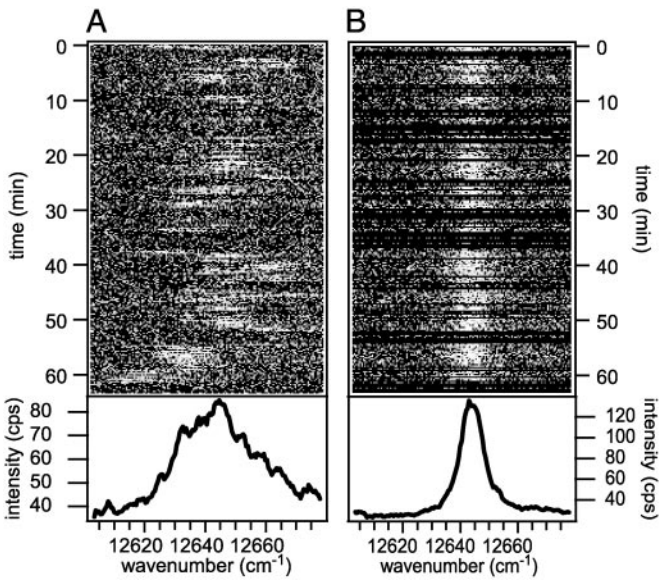

Fig. 3. Small spectral fluctuations of an absorption. (*A*) Stack of 256 fluorescence-excitation spectra, from a narrow spectral region of Fig. 2*A* at an expanded view around the position of line a′. The fluorescence intensity is indicated by the grayscale. The average absorption line of all spectra is shown in *Lower* and shows a linewidth of 41.6 cm^{-1} (full width at half maximum). (*B*) Stack of 172 fluorescence-excitation spectra that were obtained after fitting each individual scan to a Lorentzian profile and subsequently shifting the individual scans so that the peak positions of the fits coincided. The spectrum in *Lower* displays the average of all scans and features a width of 7.5 cm^{-1} (full width at half maximum).

$\approx 2 \times 10^{-2}$ s^{-1} for the absorptions of complex 1 and $\approx 10^{-3}$ s^{-1} for the absorptions of complex 2.

In addition to the spectral jumps of several hundred wavenumbers, we observed also smaller spectral shifts on a faster time scale. This observation is illustrated in Fig. 3, which shows an expanded view of the spectral region around the absorption (Fig. 2*A*, a′). In *A*, the raw data are shown in a similar representation as they were shown previously, and the width of the transition in the averaged spectrum is 41.6 cm^{-1} (full width at half maximum). From the data, it is evident that the observed linewidth of the averaged spectrum results predominantly from the accumulation of smaller spectral changes. By fitting the spectrum in every single sweep to a Lorentzian profile, it was determined that, for this example, the peak position changed on average by 4.7 cm^{-1} per scan of 15-s duration. Similar values are observed for the other transitions (Table 1). To obtain the spectrum in Fig. 3*B*, the individual scans have been shifted so that the fitted peak positions coincide, and subsequent averaging uncovers a width of 7.5 cm^{-1} (full width at half maximum) for this absorption. In other cases, the same procedure yields linewidths of 4–12 cm^{-1} (Table 1). Clearly, we cannot exclude additional contributions to the linewidth, which may stem from faster unresolved spectral dynamics of the chromophore while the laser scanned through the resonance. However, the observed values cover the same range as those reported for the homogeneous linewidth of the B800 absorptions (19, 26), restricting additional contributions to the line broadening to ≈ 1 cm^{-1} or less. Given the scan speed of the laser, the underlying processes have to occur within <200 ms. In general, the data show a clear correlation between the widths of the spectral fluctuations and the related time scales: the smaller that the spectral movements are, the faster the rate will be at which they occur. However, it should be noted that this approach does not permit us to observe small spectral shifts that

Table 1. Properties of the absorptions from complexes 1 and 2

	Complex 1				Complex 2					
Label	a	a′	b	b′	a	a′	b	b′	c	c′
Spectral position, cm^{-1}	12921	12643	12753	12494	12928	12587	12754	12484	12698	12518
Difference in spectral position, cm^{-1}	278	278	259	259	341	341	270	270	180	180
Rate, s^{-1}	1.5×10^{-2}	1.9×10^{-2}	2×10^{-2}	2.2×10^{-2}	5×10^{-4}	2×10^{-3}	5.5×10^{-3}	1×10^{-3}	8.3×10^{-3}	1.3×10^{-3}
Observed linewidth, cm^{-1}	36.8	41.6	28.5	29.1	39.1	21.1	11.2	28.5	70.3	46.7
Average spectral change per scan, cm^{-1}	3.5	4.7	4.5	5.9	5.3	5.4	6.8	3.9	6.0	3.6
Processed linewidth, cm^{-1}	7.4	7.5	5.9	11.5	11.3	7	3.9	4.7	5	5
Scantime across linewidth, ms	150	180	130	240	230	150	80	100	100	100

For each absorption line the following properties are listed: spectral position, mutual spectral distance between the two anticorrelated line positions, average rate at which the absorption fluctuates between the two anticorrelated spectral positions, linewidth observed in the averaged spectrum, average spectral change of the peak position per scan, linewidth of the averaged spectrum after data processing as described in the text, and time required to scan the laser through the processed linewidth.

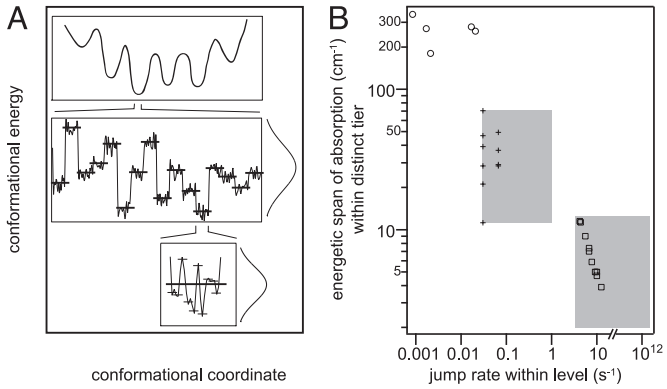

Fig. 4. (*A*) Schematic illustration of three subsequent tiers of the potential energy hypersurface of a protein as a function of an arbitrary conformational coordinate. (*B*) Width of the spectral region that is covered by the spectral fluctuations of the chromophore within a certain time window, termed energetic span, versus the rate of these fluctuations in the three tiers that were found. For details see *Discussion*.

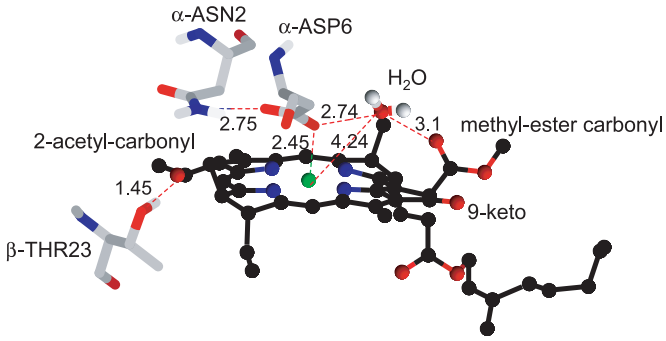

Fig. 5. Part of the binding pocket for a B800 BChl *a* molecule in *Rs. molischianum* (blue, N; red, O; green, Mg). Dashed lines indicate likely hydrogen bonds and metal ligands at short distances (Å).

occur at slow rates or to resolve shifts significantly smaller than the homogeneous linewidth of the optical transition at any rate.

Discussion

From spectral hole-burning experiments on LH2 from *Rhodopseudomonas acidophila*, it is known that relative distance changes of $\Delta R/R \approx 10^{-4} - 10^{-2}$ are already sufficient to result in spectral shifts of 1–100 cm^{-1} for the B800 absorptions (27). Consequently, we ascribe the observed spectral fluctuations to the modulations of the pigment–protein interactions in the vicinity of the chromophore, and according to the concept of CSs, we attribute the three observed categories of spectral fluctuations to the presence of at least three distinct energy tiers in the energy landscape of the protein. To address this issue in more detail, we introduce the term "energetic span" of the chromophore absorption. This term refers to the width of the spectral region that is covered by the spectral fluctuations of the chromophore within a certain time window. In Fig. 4, we have illustrated a simplified protein energy landscape along an arbitrary conformational coordinate, together with the information that we have obtained for the relationship between the energetic spans of the chromophore absorptions and the corresponding time scales. We assume that the magnitudes of the observed spectral shifts represent a hierarchy of tiers in which the average height of the energy barriers decreases from top to bottom.

The highest tier (Fig. 4*A Top*) is thought to represent specific arrangements of the atoms, such as in the protein backbone, and transitions between these levels give rise to spectral shifts of several hundred wavenumbers in the optical spectrum of the chromophore. Presumably, the spectral shift is indicative of a significant barrier height between the initial and final CS. Because the chromophore absorptions sample only a few discrete spectral positions, the energetic span covered by the pigment absorption at this level of the hierarchy was taken as the energy difference between two anticorrelated lines. The underlying processes in this tier occur at rates of 10^{-2} to 10^{-3} s^{-1}. However, each energy level in the highest tier is described more appropriately as a rugged energy surface, as shown in Fig. 4*A Middle* on an enlarged scale. Within this tier, we have indicated in Fig. 4*A Middle* the average CS energy (bold bar) and the distribution of states (smooth curve to the right). Accordingly, we ascribe the spectral changes of ≈ 5 cm^{-1} between two successively recorded chromophore spectra to structural fluctuations of the protein between two CSs inside this tier of the energy landscape. Information about the distribution of the CS energies within this level of the hierarchy is provided by the linewidth of ≈ 50 cm^{-1}, which is obtained after accumulating hundreds of individual sweeps. Boundaries for the rates of the protein dynamics that result in these spectral fluctuations can be estimated from the repetition rate of the individual laser sweeps (0.03–0.07 s^{-1}) and the time required to scan the laser across the accumulated linewidth (1 s^{-1}). The shaded rectangle in the center of Fig. 4*B* indicates these constraints, and the data points (+) are placed at the repetition rate of the experiments.

Descending further in the hierarchy, a situation is finally reached in which the protein transitions between the CSs cause only minor changes in the chromophore spectra. Certainly, the smallest detectable spectral change corresponds to a broadening, rather than a shift, of the absorption line. In Fig. 4*A Bottom*, we have illustrated a situation in which the individual CSs are already quantized in energy (light bars) and can be characterized by a statistical distribution (smooth curve to the right) around a mean value (bold bars), which represents one of the average CS energies of the next higher tier. Likely causes for the CS within this tier are vibrational and/or librational degrees of freedom of the protein. Within the temporal resolution of our experiment, all CSs of this tier are sampled. A lower boundary for the rate of the processes that are able to contribute to unresolved spectral dynamics hidden in the residual linewidth of the B800 absorptions is provided by the time that is required to scan the laser across this linewidth. Therefore, the maximum possible energetic span for the chromophore absorptions and vice versa (the smallest possible rate for dynamical processes in the protein) can be extracted from the broadest processed linewidth. These boundaries fix the upper left corner of the shaded rectangle at the lower right of Fig. 4*B*. It should be mentioned that an upper boundary for the rate of these processes follows from the Fourier transform of the linewidth itself, which yields $\approx 10^{12}$ s^{-1}. However, our approach is inappropriate to monitor the ultrafast dynamical processes, and it focuses on those dynamical processes that occur at very low rates. Accordingly, the possible parameter combinations in the lowest observable hierarchical level are restricted to the area indicated by the shaded rectangle at the bottom of Fig. 4*B*. The data points (□) correspond to the processed linewidth versus the reciprocal scan time of the laser. Certainly, Fig. 4*B* provides only a crude picture. In addition, it should be kept in mind that this method does not permit us to distinguish small spectral changes occuring at fast rates from small spectral changes occuring at slow rates. However, large spectral shifts at fast rates have not been observed, and the data points in Fig. 4*B* should be read as a boundary for the possible parameter combinations. Only combinations of rates and spectral shifts below the diagonal of the diagram are compatible with the observations.

BIOPHYSICS

An intriguing question that arises is whether the observed spectral shifts can be related to structural rearrangements in the binding pocket of the chromophore, which is shown in Fig. 5. It is known from theoretical work that the Q_y transition of BChl *a* is very sensitive to perturbation of the π-conjugation system of the bacteriochlorin macrocycle and also is affected by the ligands to the central Mg atom. For instance, an out-of-plane rotation of the C_2 acetyl group with respect to the bacteriochlorin plane yields a blue shift of the pigment transition of up to 500 cm^{-1} (28). A deviation from planarity of BChl will have similar effects. Density functional theory calculations that examined the ligand binding of the BChl *a* central Mg atom to the charged α-Asp-6 amino acid in the B800 binding pocket of *Rs. molischianum* estimated a red shift of 190 cm^{-1} (29) for the site energy of a BChl *a* molecule in the B800 ring.

We infer that the observed spectral variations result from local conformational changes that affect the π-conjugation system of the bacteriochlorin macrocycle, for example, by affecting the planarity of the ring, reorienting side groups, or rearranging the central-Mg atom and its ligands. In this regard, several aspects have to be considered. First, the huge spectral changes might reflect fluctuations in the strength of a hydrogen bond between the β-Thr-23 amino acid and the C_2 acetyl group of the BChl *a* molecule (18, 25). This interpretation is evidenced by site-directed mutagenesis on LH2 from *Rhodobacter sphaeroides* (30, 31). For this species, a β_{-10}-Arg amino acid is hydrogen bonded to the C_2 acetyl carbonyl group of the BChl *a* molecule, and spectral shifts of 100–200 cm^{-1} for the B800 absorption maximum are observed if this amino acid is substituted by a non-hydrogen bonding residue. Second, the polarity of the B800 binding site might be of influence, as indicated by shifts of up to 300 cm^{-1} for the spectra from monomeric BChl *a* on solution in various organic solvents (32). For *Rs. molischianum*, the x-ray structure shows a water molecule in close proximity to the α-Asp-6 and the methyl ester carbonyl of the BChl *a* that might cause variations in the electrostatic environment of the pigment (18). Electrostatic interactions with water molecules or other polar groups at a distance away from the BChl *a* binding pocket will be of no great influence to the spectral characteristics of the chromophore because such interactions depend strongly on distance. Moreover, electrostatic effects depend on the change of the effective dipole moment, $f \cdot \Delta\mu$, on excitation of BChl *a*, which is only $\approx$1 D. In summary, it appears very reasonable that the observed spectral shifts result from structural fluctuations within the binding pocket of the chromophore.

Employing single-molecule spectroscopic techniques allowed us to elucidate the organization of the protein energy landscape in hierarchical tiers. In addition, a clear correlation for the transition rates between those states and the energy separation of the levels involved is uncovered. This approach avoids the lack of synchronization that is inherent to conventional ensemble techniques and yields a valuable tool for an experimental verification of concepts that are essential for the development of a universal model for the conformational dynamics of protein folding.

We thank Cornelia Münke for excellent technical assistance. This work was supported by the Volkswagen Foundation within the framework of the priority area "Physics, Chemistry and Biology with Single Molecules."

1. Frauenfelder, H., Sligar, S. G. & Wolynes, P. G. (1991) *Science* **254,** 1598–1603.
2. Nienhaus, G. U. & Young, R. D. (1996) in *Encyclopedia of Applied Physics* (VCH, New York), Vol. 15, pp. 163–184.
3. Frauenfelder, H., Nienhaus, G. U. & Young, R. D. (1994) in *Disorder Effects in Relaxational Processes*, eds. Richert, R. & Blumen, A. (Springer, Berlin), pp. 591–614.
4. Frauenfelder, H. & McMahon, B. H. (2001) in *Single Molecule Spectroscopy*, eds. Rigler, R., Orrit, M. & Basché, T. (Springer, Berlin), pp. 257–276.
5. Frauenfelder, H., McMahon, B. H., Austin, R. H., Chu, K. & Groves, J. T. (2001) *Proc. Natl. Acad. Sci. USA* **98,** 2370–2374.
6. Leeson, D. T., Wiersma, D. A., Fritsch, K. & Friedrich, J. (1997) *J. Phys. Chem. B* **101,** 6331–6340.
7. Fritsch, K., Friedrich, J., Parak, F. & Skinner, J. L. (1996) *Proc. Natl. Acad. Sci. USA* **93,** 15141–15145.
8. Parak, F. & Nienhaus, G. U. (2002) *Chemphyschem* **3,** 249–254.
9. Mourant, J. R., Braunstein, D. P., Chu, K., Frauenfelder, H., Nienhaus, G. U., Ormos, P. & Young, R. D. (1993) *Biophys. J.* **65,** 1496–1507.
10. McMahon, B. H., Müller, J. D., Wraight, C. A. & Nienhaus, G. U. (1998) *Biophys. J.* **74,** 2567–2587.
11. Austin, R. H., Beeson, R. W., Eisenstein, L., Frauenfelder, H. & Gunsalus, I. C. (1975) *Biochemistry* **14,** 5355–5373.
12. Schlichter, J. & Friedrich, J. (2001) *J. Chem. Phys.* **114,** 8718–8721.
13. Fritsch, K., Eicker, A., Friedrich, J., Kharlamov, B. M. & Vanderkooi, J. M. (2002) *Europhys. Lett.* **41,** 339–344.
14. Skinner, J. L., Friedrich, J. & Schlichter, J. (1999) *J. Phys. Chem. A* **103,** 2310–2311.
15. Pullerits, T. & Sundström, V. (1996) *Acc. Chem. Res.* **29,** 381–389.
16. Cogdell, R. J., Isaacs, N. W., Howard, T. D., McLuskey, K., Fraser, N. J. & Prince, S. M. (1999) *J. Bacteriol.* **181,** 3869–3879.
17. Hu, X., Ritz, T., Damjanovic, A., Autenrieth, F. & Schulten, K. (2002) *Q. Rev. Biophys.* **35,** 1–62.
18. Koepke, J., Hu, X., Münke, C., Schulten, K. & Michel, H. (1996) *Structure (London)* **4,** 581–597.
19. van Oijen, A. M., Ketelaars, M., Köhler, J., Aartsma, T. J. & Schmidt, J. (2000) *Biophys. J.* **78,** 1570–1577.
20. Tietz, C., Chekhlov, O., Dräbenstedt, A., Schuster, J. & Wrachtrup, J. (1999) *J. Phys. Chem. B* **103,** 6328–6333.
21. Hofmann, C., Ketelaars, M., Matsushita, M., Michel, H., Aartsma, T. J. & Köhler, J. (2003) *Phys. Rev. Lett.* **90,** 013004.
22. van Oijen, A. M., Ketelaars, M., Köhler, J., Aartsma, T. J. & Schmidt, J. (1999) *Science* **285,** 400–402.
23. Ketelaars, M., van Oijen, A. M., Matsushita, M., Köhler, J., Schmidt, J. & Aartsma, T. J. (2001) *Biophys. J.* **80,** 1591–1603.
24. Monshouwer, R., Abrahamsson, M., van Mourik, F. & van Grondelle, R. (1997) *J. Phys. Chem. B* **101,** 7241–7248.
25. Germeroth, L., Lottspeich, F., Robert, B. & Michel, H. (1993) *Biochemistry* **32,** 5615–5621.
26. de Caro, C. A., Visschers, R. W., van Grondelle, R. & Völker, S. (1994) *J. Phys. Chem.* **98,** 10584–10590.
27. Zazubovich, V., Jankowiak, R. & Small, G. J. (2002) *J. Phys. Chem. B* **106,** 6802–6814.
28. Gudowska-Novak, E., Newton, M. D. & Fajer, J. (1990) *J. Phys. Chem.* **94,** 5795–5801.
29. He, Z., Sundström, V. & Pullerits, T. (2002) *J. Phys. Chem. B* **106,** 11606–11612.
30. Gall, A., Fowler, G. J. S., Hunter, C. N. & Robert, B. (1997) *Biochemistry* **36,** 16282–16287.
31. Fowler, G. J. S., Visschers, R. W., Grief, G. G., van Grondelle, R. & Hunter, C. N. (1992) *Nature* **355,** 848–850.
32. Limantara, L., Sakamoto, S., Koyama, Y. & Nagae, H. (1997) *Photochem. Photobiol.* **65,** 330–337.